



**HAL**  
open science

## Solidification of Polyurethane Model Foams via Catalyst Drainage from a Secondary Foam

Manon Jouanlanne, Antoine Egelé, Wiebke Drenckhan, Jean Farago, Aurélie Hourlier-fargette

► **To cite this version:**

Manon Jouanlanne, Antoine Egelé, Wiebke Drenckhan, Jean Farago, Aurélie Hourlier-fargette. Solidification of Polyurethane Model Foams via Catalyst Drainage from a Secondary Foam. *Macromolecular Rapid Communications*, In press, 10.1002/marc.202400254 . hal-04682582

**HAL Id: hal-04682582**

**<https://hal.science/hal-04682582v1>**

Submitted on 30 Aug 2024

**HAL** is a multi-disciplinary open access archive for the deposit and dissemination of scientific research documents, whether they are published or not. The documents may come from teaching and research institutions in France or abroad, or from public or private research centers.

L'archive ouverte pluridisciplinaire **HAL**, est destinée au dépôt et à la diffusion de documents scientifiques de niveau recherche, publiés ou non, émanant des établissements d'enseignement et de recherche français ou étrangers, des laboratoires publics ou privés.



Distributed under a Creative Commons Attribution 4.0 International License

# Solidification of Polyurethane Model Foams via Catalyst Drainage from a Secondary Foam

Manon Jouanlanne, Antoine Egelé, Wiebke Drenckhan, Jean Farago, and Aurélie Hourlier-Fargette\*

Due to their unique mechanical and thermal properties, polyurethane foams are widely used in multiple fields of applications, including cushioning, thermal insulation or biomedical engineering. However, the way polyurethane foams are usually manufactured - via chemical foaming - produces samples where blowing and gelling occur at the same time, resulting in a morphology control achieved by trial and error processes. Here, a novel strategy is introduced to build model homogeneous polyurethane foams of controlled density with millimetric bubbles from liquid templates. By producing a polyurethane foam via physical bubbling without a catalyst and gently depositing a secondary foam containing catalyst on the top of this first foam, it is possible to take advantage of drainage mechanisms to trigger the solidification of the bottom foam. The characterization of the samples performed by X-ray microtomography allows to study quantitatively the structure of the final solid foam, at the global and at the local scale. Using the tomographic 3D images of the foam architectures, the superimposed foam technique introduced in this article is shown to be promising to produce foams with a good homogeneity along the vertical direction, with a density controlled by varying the concentration of catalyst in the secondary foam.

have been investigated,<sup>[2]</sup> including various hydrogels<sup>[5]</sup> but also polyurethanes.

More precisely, in the pioneering work towards templated polyurethane foams of Aouatef Testouri et al.,<sup>[6]</sup> the use of microfluidics decouples the foaming and the solidification of the foam by a progressive introduction of the different compounds (polyol, surfactant, catalyst, and isocyanate) in a microfluidic chip. The chip comprises mixing units and takes advantage of the presence of the bubbles to enhance mixing. This strategy is very different from the classical foaming techniques of polyurethane,<sup>[7,8]</sup> which rely on two chemical reactions: the reaction of isocyanate with polyol (gelling reaction, that builds urethane bonds) and the reaction of water with isocyanate (blowing reaction, that produces CO<sub>2</sub> that feeds the bubbles). Such chemical foaming is widely used in the industry for multiple applications,<sup>[9]</sup> associated to interesting mechanical, thermal and acoustic properties that are directly linked to the structure of those cellular materials.<sup>[10]</sup>

## 1. Introduction

Tailoring solid foam architectures by controlling the structure of their liquid foam precursors is a field that has been attracting a growing interest over the past decade,<sup>[1,2]</sup> referred to as *liquid foam templating*. Such techniques allow to produce model foams by a control of the bubble sizes (as well as of their polydispersity<sup>[3,4]</sup>) and of the key parameters that influence pore opening mechanisms and set the liquid fraction - and thus the density of the resulting solid cellular systems. Multiple materials

However, the development of a fundamental understanding of the mechanisms determining the evolution of the foam morphology during such chemical foaming processes is still in progress.<sup>[11]</sup> With chemical foaming, the growth of bubbles and the solidification occur at the same time, leading, for instance, to anisotropy of the resulting cellular materials.<sup>[12]</sup>

Within the liquid foam templating framework, working with a bottom up approach (rather than with a top down approach, as in classical chemical foaming) allows to reach a high level of control on foam architectures. Bubbles are produced one by one in the liquid state, and most of the general morphology parameters of the foam are determined when the foam is still liquid, before solidification occurs. This allows to decouple the generation and solidification steps, to reach very monodisperse foams, with no anisotropy in terms of cell shapes, and to access a wide range of bubble sizes through a relevant choice of physical bubbling mechanisms. This decoupling allows a better understanding and control of the resulting morphologies than in chemical foaming, where a whole range of complex mechanisms occurs at the same time.

In the present work, we develop an experimental approach towards the generation of polyurethane model foams with millimetric bubbles from a mixture of polyol, surfactant, catalyst, and

M. Jouanlanne, A. Egelé, W. Drenckhan, J. Farago, A. Hourlier-Fargette  
 Université de Strasbourg, CNRS, Institut Charles Sadron UPR22  
 Strasbourg F-67000, France  
 E-mail: [hourlierfargette@unistra.fr](mailto:hourlierfargette@unistra.fr)

 The ORCID identification number(s) for the author(s) of this article can be found under <https://doi.org/10.1002/marc.202400254>

© 2024 The Author(s). Macromolecular Rapid Communications published by Wiley-VCH GmbH. This is an open access article under the terms of the [Creative Commons Attribution](https://creativecommons.org/licenses/by/4.0/) License, which permits use, distribution and reproduction in any medium, provided the original work is properly cited.

DOI: 10.1002/marc.202400254

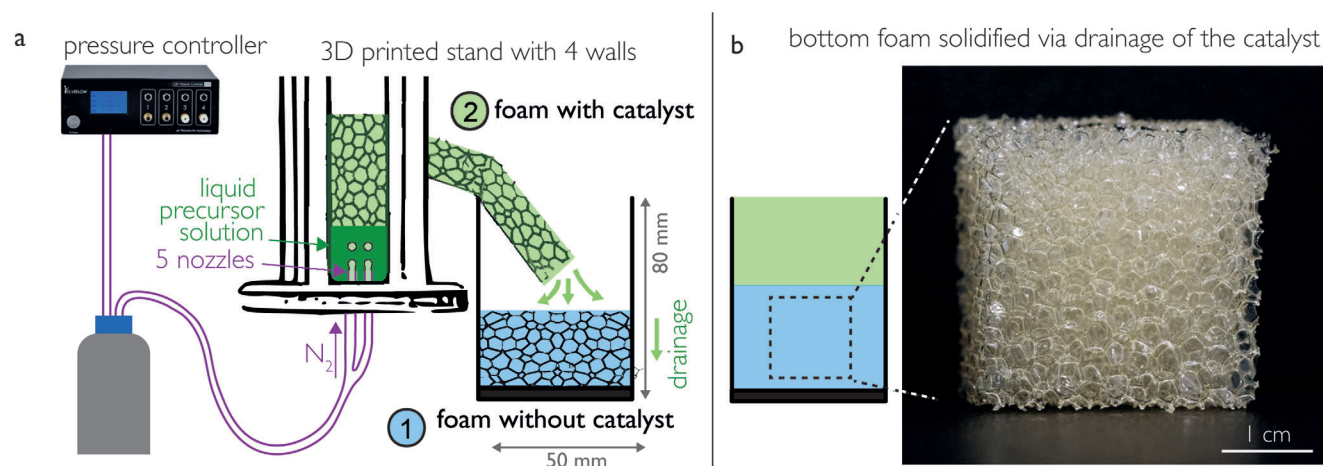


**Figure 1.** Experimental setup: a) Bubbles are generated by blowing nitrogen through nozzles at constant pressure into a precursor blend of polyurethane, first without catalyst for the first foam, labelled (1) on the schematic, then with catalyst for the secondary foam, labelled (2) on the schematic. The catalyst then drains from the top foam into the bottom foam, triggering the solidification of the bottom foam. b) All foams analysed in this article are extracted from the bottom foam (in blue), which is solidified by drainage of the catalyst from the top foam.

isocyanate, to match the two following criteria: we aim for foams (i) which are homogeneous in terms of bubble sizes and structure thicknesses, and (ii) with architectures dictated by capillarity (i.e., which follow Plateau's rules<sup>[13,14]</sup>) in the liquid state, that are conserved upon solidification. We are specifically interested in the way the catalyst is introduced to trigger the solidification of the structures once they have reached mechanical equilibrium.

While catalysis strategies have been largely studied from a chemical point of view,<sup>[15]</sup> we propose here an alternate method based on a physical approach, taking advantage of one of the key mechanisms in foam ageing: drainage of liquid foams, corresponding to a downward flow of liquid in the continuous matrix, caused by gravity.<sup>[14,16]</sup> This usually results in a gradient in liquid fraction, which is well understood both experimentally and theoretically,<sup>[14]</sup> and has also been investigated in the context of complex fluids.<sup>[17]</sup> To go further and consider stationary drainage, the concept of forced drainage<sup>[18]</sup> consists in reinjecting liquid at the top of a foam, and studying the resulting liquid fraction profile. Here we propose a strategy of solidification inspired by this forced drainage technique (**Figure 1**) and based on the propagation of the catalyst from a secondary foam - with catalyst - placed on top of a first foam which is produced without catalyst. Drainage, rather than diffusion, is the key mechanism underlying the propagation of the catalyst. The advantage of introducing the draining material as a secondary foam, rather than as a bulk liquid, is to avoid an inhomogeneous drainage and ensure a better homogeneity of the samples: if a dense liquid was superimposed directly onto the light foam, the liquid would flow mainly through preferred channels (this inhomogeneity of the flow is similar to what is observed in the case of a Rayleigh-Taylor instability). We show that the superimposed foam technique triggers the solidification successfully, and that a fine control of the experimental parameters allows to produce foams with no significant gradient of thicknesses of the structures due to gravity, and with a density controlled by the concentration of catalyst in the top foam. Figure S1 (Supporting Information) presents images of a foam obtained with a single foaming step, to emphasize by compari-

son the interest of the strategy shown in the current work (superimposed foam technique) in improving the vertical homogeneity and allowing to retain a structure following Plateau's laws.

## 2. Experimental Section

### 2.1. Polyurethane Precursor Solutions

The precursor solution of polyurethane was composed of polyols, isocyanate, surfactant—and catalyst for the secondary foam—with a formulation inspired from ref. [6]. Part A of the precursor comprises polyols, surfactant, and catalyst, and Part B the isocyanate only. The mixing of Part A and Part B was performed just before foaming. To reduce the viscosity of the foaming solution, a mixture of two polyols was used, as a little proportion of low viscosity polyol induced a drastic change in the viscosity of the mixture<sup>[19]</sup>: the low molecular polyol tripropylene glycol (TPG, 97% by Sigma-Aldrich) (10 wt.% of Part A) was mixed with a trifunctional polyether polyol Lupranol 2090 (provided by BASF Polyurethanes GmbH) (base of Part A). The surfactant used was a PDMS-PEO block-co-polymer surfactant Tegostab B8002 (Evonik Industries) (5 wt.% of Part A), and the catalyst was a tertiary-amine based catalyst, Jeffcat ZR50 (Huntsmann Corporation) (0 wt.% to 0.1 wt.% of Part A). Part B was an oligomeric form of methylene diphenyl diisocyanate (MDI) Lupranat M20S (provided by BASF Polyurethanes GmbH), and the ratio between Part B and Part A was 0.288(B):1(A). In some cases, 0.05 g of polyurethane black dye (Smooth-On SO-Strong Black) was added to visualize the flow.

Mixing steps were performed either by hand (samples with 0.0125, 0.05 and 0.1 wt.% of catalyst) or with an IKA Ultra-Turrax disperser to increase reproducibility and test the influence of the mixing (samples with 0.025 wt.% of catalyst). With the IKA Ultra-Turrax disperser, first, the polyols were mixed at speed 2 ( $\approx 1000$  rpm) for 5 min, then degassed overnight in a vacuum oven (30 °C,  $-90$  kPa). Next, the surfactant and catalyst were added and mixed for 1 min at speed 2. Finally, the isocyanate was

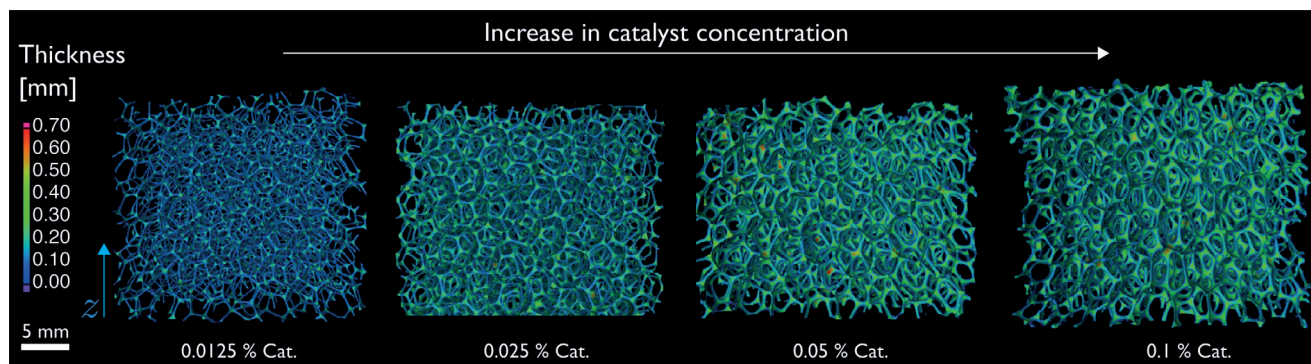


**Figure 2.** Tomographic images of primary (bottom) foams obtained with different catalyst concentrations in the secondary (top) foams: foams with four different formulations are produced as described in the Experimental section. The bottom foam has no catalyst and the secondary foam is prepared with, from left to right, a concentration of Jeffcat ZR50 of 0.0125, 0.025, 0.05, and 0.1 wt.% of Part A. The structure thicknesses are extracted with VG Studio MAX software, and shown here with the color code presented at the left of the image. Those tomographic images highlight the increase in thickness and thus in density of the foams when the catalyst concentration of the secondary foam is increased – at constant bubble size.

added and mixed for 5 min at speed 2. Note that experiments involving isocyanates required to be carried out carefully in a fume hood, with samples left under the fume hood for several days until full reaction of the isocyanates with either the polyols or the ambient humidity. The viscosity of Part A was measured at 20 °C using a DHR3 rheometer from TA Instruments with a cone-plate geometry and found to be  $1.02 \pm 0.01$  Pa·s over a range of shear rates going from 0.1 to 1000  $s^{-1}$ .

## 2.2. Foaming Protocol

Nitrogen was blown into 40 mL of foaming solution at constant pressure (100 mbar) using an Elveflow OB1 MK3+ pressure controller, via five nozzles of inner diameter 150  $\mu$ m connected to an aluminium tank under pressure (Figure 1a). The produced foam flowed down along a ramp made of a PVC sheet with a U-shaped cross-section before dripping into a container. The production of the foam was divided into two steps. The first step consisted in producing a foam without catalyst, which was placed at the bottom of the container. The second step consisted of replacing the foaming solution by a solution with catalyst (from 0.0125 to 0.1 wt.%), and producing a second foam that was gently poured onto the first one using also a PVC sheet as a ramp. The time of introduction of the second foam was comprised between 5 and 13 min after the end of the preparation of the first foam in all the experiments. The production time for each foam was of the order of 10 min, the foam was generated by bubbling and continuously deposited in the container via the PVC ramp. The temporal aspects may be important to control even better, as they determine the initial state of the bottom foam, as well as the viscosity of the secondary foam containing catalyst (that increased as the solidification process was initiated). It was noticed that temperature and humidity may also affect the results, as a change in temperature affects the viscosity of both foams, and a change in humidity may induce a reaction between isocyanates and water coming from the environment, resulting in unwanted small bubbles in the matrix, and that the stability of the foam seemed to be affected by the ageing of the chemicals. All those parameters are

important to control carefully in order to be able to obtain reproducible foams.

## 2.3. X-Ray Tomography Characterization

For each experiment, after solidification, a cubic sample with sides of  $32 \pm 3$  mm was cut from the bottom foam (highlighted in blue in Figure 1b) using a thermocut (Proxxon). Each sample was scanned with the X-ray microtomograph EasyTom 150/160 from RX Solutions to provide a 3D characterization, and stacks of images were transferred into Xact software to reconstruct 3D structures, that were then imported into VG Studio MAX 2023.1 software for visualization and analysis (Figure 2). All tomographies were performed at a resolution of 25  $\mu$ m (average scanning time of  $\approx 2$  h). Extraction of bubble sizes was performed using the Foam/powder analysis tool from VG Studio, with a sensibility threshold of 35 % for the detection of boundaries between bubbles. Extraction of strut and vertex thicknesses was performed using the same Foam/powder analysis module, followed by the process illustrated in Figure 3 to extract the strut thickness  $w_s$  and the vertex thickness  $w_v$ , for which additional details are given in Section 3. Figure 3 shows the Probability Density Function (PDF) of the structure thickness normalized by the mean structure thickness, defined as the histogram of  $w/\langle w \rangle$  where each bin count was divided by  $(N_{\text{tot}} * \delta n)$ , where  $N_{\text{tot}}$  is the total number of counts and  $\delta n$  is the bin width. This definition ensures that a numerical integration gives always one whatever the choice of  $\delta n$ . The raw structure thickness data were obtained from the VG Studio analysis tool, using a method based on growing spheres inside the polyurethane matrix. Additional images from the bubble size/thickness analysis are shown in the Figure S2 (Supporting Information).

In addition to the information extracted from VG Studio, the topological network of struts was extracted via a purpose-designed Matlab program, inspired by refs. [20, 21]. This home-made program performed a skeletonisation of the 3D images, found the nodes of the foam and created a skeleton composed of straight line struts linking those nodes. From the extracted



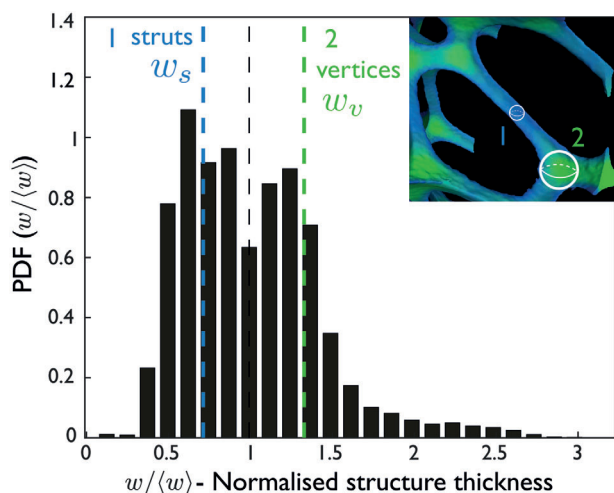


**Figure 3.** Distribution of the thicknesses in the foam architecture: Example of the Probability Density Function (PDF) normalized distribution function of the structure thicknesses measured on the tomographic images with the software VG Studio MAX, for a polyurethane bottom foam produced using a secondary foam with a catalyst concentration of 0.025 wt.%. We observe two peaks in the distribution, corresponding respectively to the vertex and to the strut thicknesses. The inset shows a zoom on a cell, with thin structures highlighted in blue and thicker structures in green. The histogram is divided (manually) in two parts to distinguish those two objects, with the separation highlighted by a dashed black line in the figure. The average thickness of the struts  $w_s$  is then calculated as the mean thickness of the left side of the black line (dashed blue line) and the average thickness of the vertices  $w_v$  is calculated as the mean thickness of the right side of the black line (dashed green line).

network of struts, the values of the angles between two adjacent straight struts were computed, to analyze the difference between the structural features of the solid samples and Plateau's laws,<sup>[13]</sup> the latter being constraints imposed by capillarity in the liquid state. More details about the procedures can be found in ref. [22].

### 3. Results and Discussion

To analyze the influence of the concentration of catalyst of the secondary foam, we produce identical bottom foams, and add different secondary foams with catalyst concentrations ranging from 0.0125 to 0.1 wt.%, following the protocol described in the Experimental section. We choose to focus on one single bubble size for all foams (bottom and top foams), of  $4.0 \pm 0.3$  mm which is fixed by the pressure and geometrical parameters of our setup,<sup>[23]</sup> and does not vary significantly upon the presence of catalyst.

Figure 2 shows the 3D reconstruction of four bottom foams, obtained with the superimposed foam technique with respectively 0.0125, 0.025, 0.05, and 0.1 wt.% of catalyst. The thickness of the architectures is highlighted with the color code on the left of the figure: we can already observe with this representation a strong influence of the concentration of catalyst on the structure thickness, especially at low catalyst concentrations, as well as an homogeneity of the samples along the  $z$  axis. We are interested in quantifying those two main features: i) the influence of the catalyst concentration on the global parameters (average strut

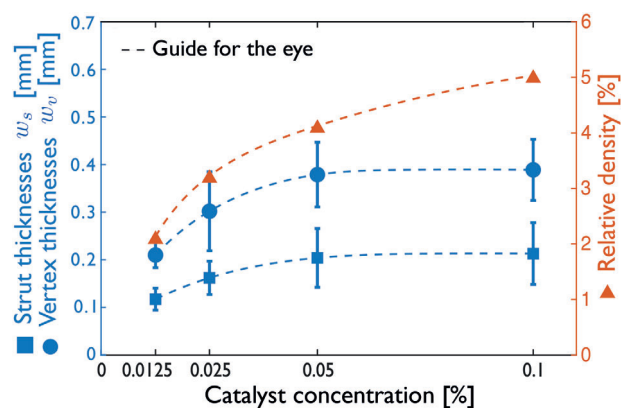


**Figure 4.** Structural characterisation of thicknesses and density: Left axis in blue: Strut thicknesses  $w_s$  and vertex thicknesses  $w_v$  as a function of the catalyst concentration in wt.%. Right axis in red: relative density of the foam as a function of catalyst concentration, extracted by weighing and measuring the volume of the cubic samples. Error bars correspond to the standard deviations of the strut and vertex thickness measured across one sample for each point.

thickness and vertex thickness), as well as ii) the details of the homogeneity along the  $z$  axis aligned with gravity. Both aspects are detailed in the subsections below.

#### 3.1. Influence of the Catalyst Concentration on the Global Foam Parameters

To obtain quantitative data on the structure thickness from the X-ray images, we extract the probability distribution function of the thicknesses obtained with the Foam/powder analysis tool of VG Studio MAX 2023.1 software. This PDF is shown in Figure 3 in a normalized way for one sample with 0.025 wt.% of catalyst, taken as an example. We observe a distribution with two peaks, one corresponding to the struts (highlighted in blue in the figure), and one corresponding to the vertices (highlighted in green in the figure). Such separation between strut and node thicknesses has already been observed in the literature on images analyzed with the same software VG Studio MAX.<sup>[24]</sup> For each sample, we extract an average strut thickness  $w_s$  calculated as the average of all thicknesses on the left of the dashed black line (separating the two peaks arbitrarily, with a placement of this dashed line performed by visual inspection of each histogram) and an average vertex thickness  $w_v$  calculated as the average of all thicknesses on the right of the dashed black line.

The structure thicknesses  $w_s$  and  $w_v$  are extracted for foams built with secondary foams of different catalyst concentrations, and represented in blue (left axis) in Figure 4. These measurements confirm the visual inspection performed on tomographic images in Figure 2, showing that the catalyst concentration has an impact on the thicknesses. We can easily understand this trend: the lower the catalyst concentration, the more time the liquid has to drain toward the bottom of the sample, resulting in a thinning of the structure. Another global parameter, the relative density of the foam, was quantified on the same samples by weighing them and measuring their volume, showing again an increase in the density with increasing catalyst

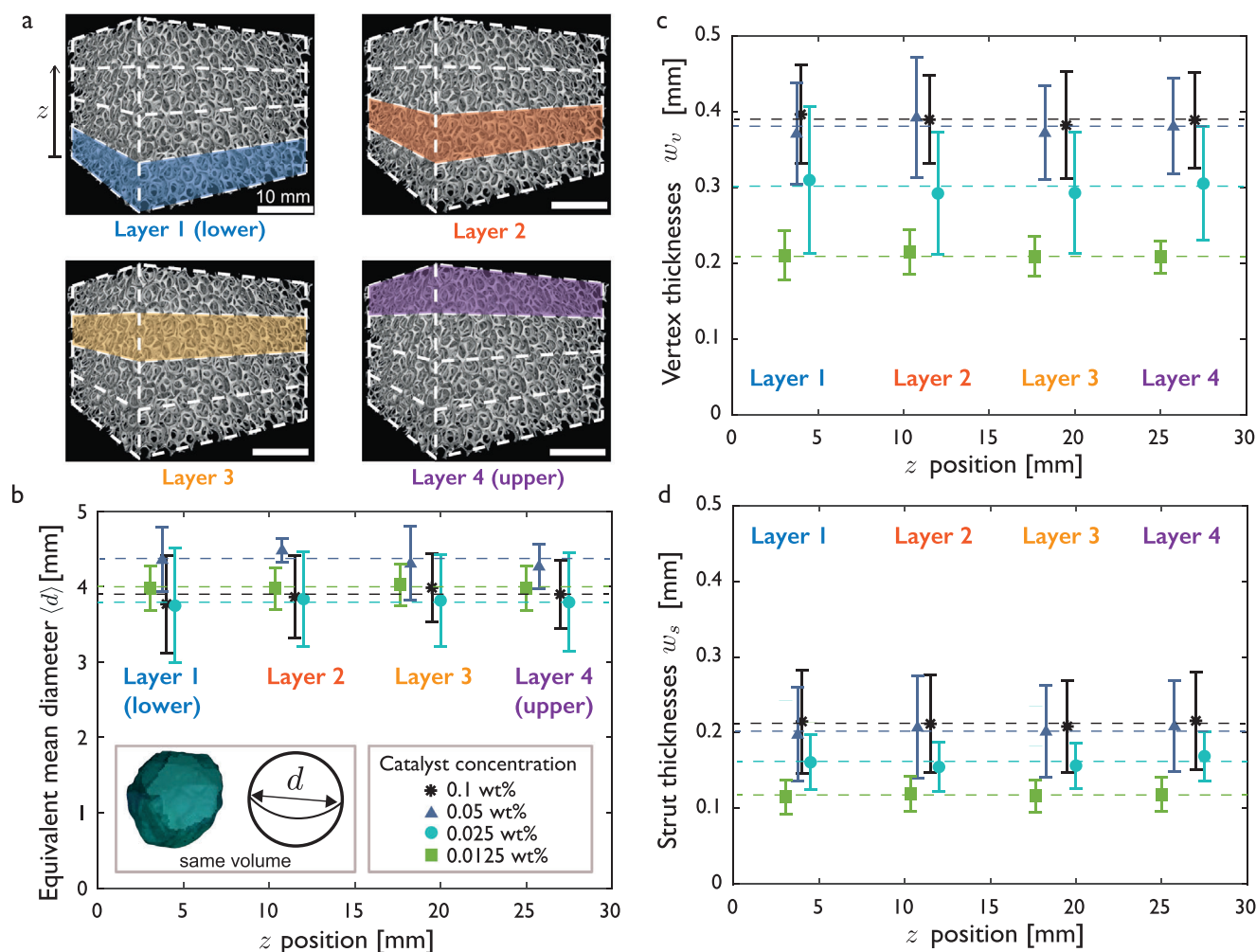


**Figure 5.** Evaluation of the homogeneity of the primary (bottom) polyurethane foams as a function of the altitude  $z$ : a) Definition of the four regions of interest studied on the primary (bottom) foams. b) Evolution of the equivalent mean bubble diameter (defined as the diameter of a sphere of the same volume as the bubble) as a function of  $z$ . Each group of points corresponds to the average over the corresponding region of interest. Four different catalyst concentrations for the secondary foam are investigated. c) Evolution of the vertex thickness (defined following the procedure described in Figure 3) as a function of  $z$ . d) Evolution of the strut thickness (defined following the procedure described in Figure 3) as a function of  $z$ . The color code in (c) and (d) is the same as in (b), and each group of points corresponds to the average over the corresponding region of interest. The error bars correspond to the standard deviations of the bubble diameter and the structure thicknesses over the corresponding region of interest. The dashed lines are guides for the eye.

concentration (right axis in red in Figure 4). Note that for high catalyst concentrations (0.05 and 0.1 wt.%) we noticed localized inhomogeneities, that may lead to small errors in the density and thicknesses which are averaged over the whole sample. Figure S3 (Supporting Information) illustrates the limits of this technique at high catalyst concentrations due to an inhomogeneous drainage because of a too fast solidification. At low catalyst concentrations, the homogeneity in the  $xy$  plane (perpendicular to the  $z$  axis along which gravity is acting) is better, but is sometimes affected by preferential drainage paths of the liquid, certainly due to an imperfect deposition of the secondary foam or the creation of preferred channels for the liquid (similar to a Rayleigh-Taylor instability). We show here a proof of concept of the technique but an improvement of some details could even reinforce homogeneity, such as an optimization of the way the secondary foam is introduced.

### 3.2. Homogeneity of the Obtained Foams Along the Vertical Direction

At a given catalyst concentration, we are interested in the variation in bubble size, strut thickness and vertex thickness along the  $z$  direction, which corresponds to the direction of drainage and gravity. Using VG Studio MAX software, we divide each sample into four regions of interest (all located on the primary (bottom) foam), corresponding to the four layers highlighted in Figure 5a. The same analysis as in the previous subsection is performed on each region of interest, providing the equivalent mean diameter (Figure 5b), the vertex thickness (Figure 5c) and the strut thickness (Figure 5d) for the four layers, on samples with four different catalyst concentrations for the secondary foam (0.0125, 0.025, 0.05, and 0.1 wt.%). We observe that with the parameters used in our experiments, we manage to reach a good homogeneity

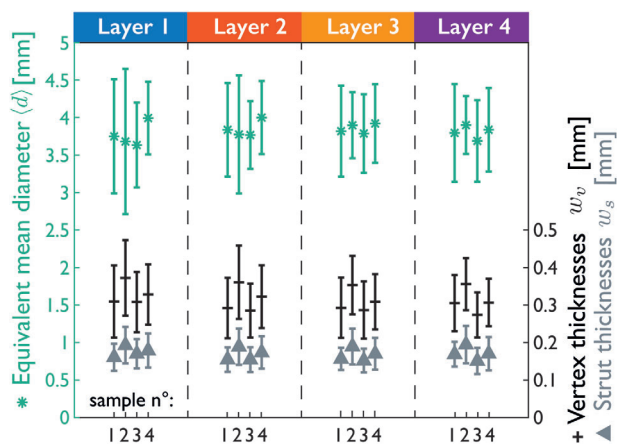


**Figure 6.** Evaluation of the reproducibility of the protocol for a catalyst concentration of 0.025 wt.%. Four identical foams were produced separately to validate that the obtained morphology is reproducible. Left axis: Mean diameter (of equivalent spheres of volume equal to the volume of the cells) at different altitudes  $z$  in the sample corresponding to the four different layers (as defined in Figure 5), for the four samples produced. Right axis: Strut thicknesses  $w_s$  and vertex thicknesses  $w_v$  for the four different layers, and for the four samples produced. Error bars correspond to the standard deviation of the measurements within each sample.

along the  $z$  axis for all three parameters. The changes in each parameter along the  $z$  axis are much smaller than the variability inside each layer, shown in Figure 5b–d with the error bars representing the standard deviations across each layer.

### 3.3. Reproducibility of the Process

We quantify the reproducibility of the process on four samples produced using the same protocol, with 0.025 wt.% concentration of catalyst in the secondary foam. Figure 6 provides the same data as Figure 5 for the four samples at 0.025 wt.% catalyst concentration, for the mean diameter (Figure 6, left axis) and strut thicknesses and vertex thicknesses on the same graph (Figure 6, right axis). This data shows that this innovative process seems to produce reproducible samples. Figure 7 is obtained using the extracted network of struts of the foam, and shows the Probability Density Function (PDF) of the strut-strut angles observed in vertices of order 4 (note that this corresponds to strut-strut angles but not to local angles, struts being approximated by straight lines in the extracted skeleton). This PDF is centered around  $109.5^\circ$ , corresponding to the angles dictated by Plateau's rules. We can remark the good reproducibility on those strut–strut angle measurements over the four samples. As a side note, we can also notice that this distribution is much closer to Plateau's rules than the samples usually obtained with chemical foaming.<sup>[21]</sup>

### 3.4. Discussion

In Figure S1 (Supporting Information), we are showing a photograph of a foam obtained without superimposition of two foams (i.e., only a “bottom” foam, but with catalyst inside). In that case, the drainage of the foam leads to a density profile and an inhomogeneity in the  $z$  direction. This is well known in the case of liquid

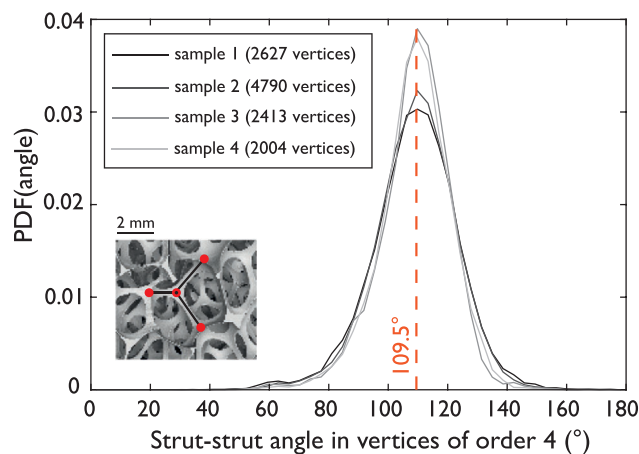


**Figure 7.** Distribution of strut angles: Probability Density Function (PDF) of the angles between pairs of struts for struts which are part of a vertex of order four, computed from the extracted network of struts in the foams, for the four samples with a catalyst concentration of 0.025 wt.% presented in Figure 6. A thin layer at the boundaries has been systematically removed from the analyses to avoid edge effects coming either from the sample itself or from the numerical protocol to extract the strut skeleton from the microtomographic reconstruction. The number of vertices taken into account in each case is specified.

foams:<sup>[25]</sup> the typical characteristic length scale over which a liquid foam is homogeneous after drainage decreases as the bubble size increases, making it impossible to obtain foams with millimetric bubbles with homogeneous thickness over several layers of bubbles after full drainage of the liquid. It is thus difficult to obtain homogeneous strut thicknesses by using only “freezing” of a liquid template after drainage.

The technique that we explore here is based on the following principles: (i) The cell size of the foams (top and bottom) is determined solely by the foaming parameters (pressure, nozzle diameter, and viscosity of the material, which is assumed to be unchanged in the initial steps of the process for the amounts of catalyst added in the formulation. The cell size of the bottom foam does not change upon introduction of the secondary foam. (ii) The bottom foam has the time to find an equilibrium (metastable) architecture (i.e., respects Plateau's laws), and (iii) when the secondary (top) foam is introduced, within the struts of the first (bottom) foam, most of the liquid in the initial foam is replaced by liquid from the secondary foam, due to the drainage mechanism. The solidification occurs as this liquid with catalyst drains into the bottom foam, and the choice of the different timescales allows to solidify the foam while this drainage process is still ongoing. We thus do not rely on the liquid fraction profiles that would be reached at long times if the foam was liquid at all times.<sup>[25]</sup>

The foams obtained have a mechanical response that is typical of elastomeric foams, with first a linear regime, followed by a plateau linked to the bending of the struts and a densification step when the cells are highly compressed.<sup>[10]</sup> This is illustrated in Figure 8, which shows the stress–strain curve under compression of two rectangular samples extracted from a primary (bottom) foam prepared with 0.025 wt.% of catalyst at two different locations (upper and lower subparts). The two subparts show a

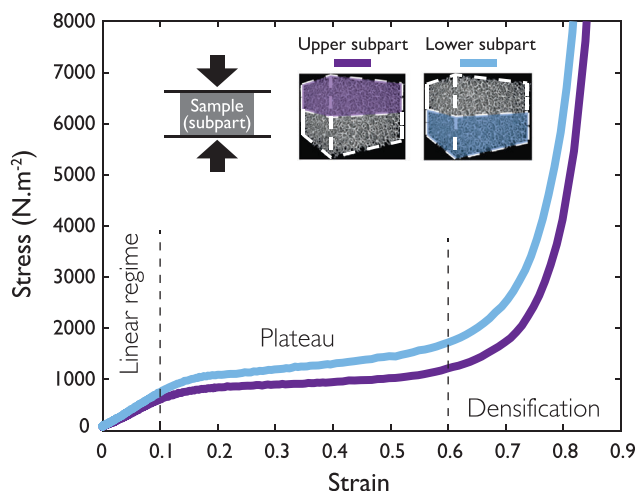


**Figure 8.** Mechanical properties: Compressive behavior of two rectangular subparts (upper subpart in dark purple and lower subpart in light blue) of a primary (bottom) foam prepared with 0.025 wt.% of catalyst in the secondary foam, highlighting the three regimes (linear regime, plateau and densification) characteristic of elastomeric foams.

similar behavior, with a linear regime up to 10% strain associated with a Young's modulus that does not differ much between the upper and lower subpart, estimated to be  $6.1 \pm 0.7$  kPa. The slight discrepancy between the two curves over the whole range explored can be explained by imperfections in the process but also most importantly by the fact that this work focuses on large bubbles and centimetric samples: this results in a ratio between the cell size and the sample size that is not ideal for mechanical characterizations, the sample being too small to be considered as a representative volume element.<sup>[26]</sup>

The goal of the process described here is to produce centimetric samples with a high level of control of the foam architectures, which allows further fundamental studies on the link between structure and properties. The question of the extension of such a strategy to industrial processes is relevant but challenging. For general cushioning materials, chemical foaming is definitely more efficient. However, to obtain fine-tuned architectures, there is no intrinsic limitation of the superimposed foam technique in terms of sample sizes in the  $xy$  plane (horizontal direction). In the  $z$  direction, achieving a constant thickness over much larger samples might be more difficult and require additional work on the details of the drainage mechanism. In addition, the accessible density range could be extended even further by also varying the bubble size, extending the range of potential applications.

## 4. Conclusion

To go beyond the limitations of classical chemical foaming for polyurethanes, we have developed in this work a novel strategy to produce model polyurethane foams that exploits drainage mechanisms under gravity, with the advantage of avoiding the creation of preferred pathways for the liquid (similar to a Rayleigh-Taylor instability). The careful choice of geometric parameters, formulations, and time scales, leads to the obtention of monodisperse polyurethane foams with millimetric bubbles with no significant thickness variations in the  $z$  direction. More precisely, the

drainage of a secondary foam containing catalyst into a first foam with no catalyst - that can thus reach its equilibrium architecture before solidification - is a promising route toward a better control of important foam parameters. This work focuses on the fabrication of model foams with samples of centimetric sizes, at a lab (desktop) scale. The main fundamental interest of such model foams is to reach a better understanding of the link between structure and properties of such architected materials. The adaptability of this technique in terms of industrial processes (both in terms of preparation efficiency, cost, and sample size) is certainly challenging and will depend on the level of control required for the foam architecture for specific applications.

The extension of the process to other bubble size ranges, and other formulations (e.g., hydrogels) is certainly possible, to provide additional tools to the foam templating techniques with a larger range of densities accessible. In addition, polyurethane foams are also used as sacrificial templates, for instance, for metallic foams,<sup>[27]</sup> which could also benefit from a higher level of control of the template architectures.

## Supporting Information

Supporting Information is available from the Wiley Online Library or from the author.

## Acknowledgements

The authors are grateful to Martin Hamann for his help with the polyurethane formulation, to Le Quan Ngo for preliminary tests that included mixing techniques for the preparation of precursor solutions, to Damien Favier for his help with the mechanical characterization of the initial formulations, to Leandro Jacomine for his help with the rheological characterizations (viscosity of liquid precursor and compression behavior of solid foams) and to Thierry Roland and the whole MIM team of Institut Charles Sadron (ICS) for fruitful discussions. This work benefited from the tools and expertises of the ICS MINAMEC Platform. The authors also thank BASF for providing chemicals used in this project. This work of the Interdisciplinary Institute HiFunMat, as part of the ITI 2021-2028 program of the University of Strasbourg, CNRS and Inserm, was supported by IdEx (Initiative d'Excellence) Unistra (ANR-10-IDEX-0002) and SFRI (STRAT'US project, ANR-20-SFRI-0012) under the framework of the French Investments for the Future Program. The authors also acknowledge funding from the IdEx Unistra framework (A. Hourlier-Fargette), and from the ANR (Agence Nationale de la Recherche) (FOAMINT project, ANR-23-CE06-0014-01). Wiebke Drenckhan acknowledges financial support by an ERC (European Research Council) consolidator grant (agreement 819511-METAFOAM). This research was funded, in whole or in part, by the ANR. A CC-BY public copyright license had been applied by the authors to the present document and will be applied to all subsequent versions up to the Author Accepted Manuscript arising from this submission, in accordance with the grant's open access conditions.

## Conflict of Interest

The authors declare no conflict of interest.

## Data Availability Statement

The data that support the findings of this study are available from the corresponding author upon reasonable request.



## Keywords

architected materials, drainage, foams, liquid foam templating, polyurethane

Received: April 19, 2024

Revised: June 20, 2024

Published online:

- 
- [1] C. Stubenrauch, A. Menner, A. Bismarck, W. Drenckhan, *Angew. Chem., Int. Ed.* **2018**, *57*, 10024.
- [2] S. Andrieux, A. Quell, C. Stubenrauch, W. Drenckhan, *Adv. Colloid Interface Sci.* **2018**, *256*, 276.
- [3] A. van der Net, A. Gryson, M. Ranft, F. Elias, C. Stubenrauch, W. Drenckhan, *Colloids Surf. A: Physicochem. Eng. Asp.* **2009**, *346*, 5.
- [4] S. Andrieux, W. Drenckhan, C. Stubenrauch, *Langmuir* **2018**, *34*, 1581.
- [5] I. B. Djemaa, S. Auguste, W. Drenckhan-Andreatta, S. Andrieux, *Adv. Colloid Interface Sci.* **2021**, *294*, 102478.
- [6] A. Testouri, M. Ranft, C. Honorez, N. Kaabeche, J. Ferbitz, D. Freidank, W. Drenckhan, *Adv. Eng. Mater.* **2013**, *15*, 1086.
- [7] N. Hilyard, A. Cunningham, *Low density cellular plastics: Physical basis of behaviour*, Springer Science & Business Media, Berlin, Heidelberg **2012**.
- [8] S.-T. Lee, N. S. Ramesh, *Polymeric foams: mechanisms and materials*, CRC press, Boca Raton **2004**.
- [9] M. Ionescu, *Chemistry and technology of polyols for polyurethanes*, iSmithers Rapra Publishing, **2005**.
- [10] M. F. Ashby, *Philos. Trans. R. Soc. A* **2006**, *364*, 15.
- [11] M. Hamann, S. Andrieux, M. Schütte, D. Telkemeyer, M. Ranft, W. Drenckhan, *J. Cell. Plast.* **2023**, *59*, 201.
- [12] A. T. Huber, L. J. Gibson, *J. Mater. Sci.* **1988**, *23*, 3031.
- [13] J. A. F. Plateau, *Statique expérimentale et théorique des liquides soumis aux seules forces moléculaires*, Gauthier-Villars, Paris **1873**.
- [14] I. Cantat, S. Cohen-Addad, F. Elias, F. Graner, R. Höhler, O. Pitois, F. Rouyer, A. Saint-Jalmes, *Foams: structure and dynamics*, OUP Oxford, Oxford **2013**.
- [15] A. L. Silva, J. C. Bordado, *Catal. Rev.* **2004**, *46*, 31.
- [16] D. L. Weaire, S. Hutzler, *The physics of foams*, Oxford University Press, Oxford **1999**.
- [17] M. Safouane, A. Saint-Jalmes, V. Bergeron, D. Langevin, *Eur. Phys. J. E* **2006**, *19*, 195.
- [18] D. Weaire, N. Pittet, S. Hutzler, D. Pardal, *Phys. Rev. Lett.* **1993**, *71*, 2670.
- [19] B. Zhmud, *Lube Mag* **2014**, *121*, 24.
- [20] M. D. Montminy, A. R. Tannenbaum, C. W. Macosko, *J. Cell. Plast.* **2001**, *37*, 501.
- [21] M. D. Montminy, A. R. Tannenbaum, C. W. Macosko, *J. Colloid Interface Sci.* **2004**, *280*, 202.
- [22] M. Jouanlanne, Phd thesis, University of Strasbourg, **2023**.
- [23] A. A. Kulkarni, J. B. Joshi, *Ind. Eng. Chem. Res.* **2005**, *44*, 5873.
- [24] J. S. Rathore, C. Vienne, Y. Quinsat, C. Tournier, *Weld. World* **2020**, *64*, 1367.
- [25] A. Maestro, W. Drenckhan, E. Rio, R. Höhler, *Soft Matter* **2013**, *9*, 2531.
- [26] C. Tekoglu, L. Gibson, T. Pardoen, P. Onck, *Prog. Mater. Sci.* **2011**, *56*, 109.
- [27] V. Paserin, S. Marcuson, J. Shu, D. S. Wilkinson, *Adv. Eng. Mater.* **2004**, *6*, 454.